Energy &
Environmental
Science

Measuring the Competition between Bimolecular Charge Recombination and Charge Transport in Organic Solar Cells under Operating Conditions

SCHOLARONE™
Manuscripts

Measuring the Competition between Bimolecular Charge Recombination and Charge Transport in Organic Solar Cells under Operating Conditions

Michael C. Heiber,[1, 2, *] Takashi Okubo,[3] Seo-Jin Ko,[1, 4] Benjamin R. Luginbuhl,[1, 4] Niva A. Ran,[1, 4] Ming Wang,[1, 4] Hengbin Wang,[5] Mohammad Afsar Uddin,[6] Han Young Woo,[6] Guillermo C. Bazan,[1, 4] and Thuc-Quyen Nguyen[1, 4, †]

[1]*Center for Polymers and Organic Solids, University of California, Santa Barbara, California 93106, USA*
[2]*Center for Hierarchical Materials Design (CHiMaD),*
Northwestern University, Evanston, Illinois 60208, USA
[3]*Department of Science, Kindai University, Higashiosaka, Osaka 577-8502, Japan*
[4]*Department of Chemistry and Biochemistry, University of California, Santa Barbara, California 93106, USA*
[5]*Mitsubishi Chemical Center for Advanced Materials,*
University of California, Santa Barbara, California 93106, USA
[6]*Department of Chemistry, Korea University, Seoul 136-713, Republic of Korea*
(Dated: July 11, 2018)

The rational design of new high performance materials for organic photovoltaic (OPV) applications is largely inhibited by a lack of design rules for materials that have slow bimolecular charge recombination. Due to the complex device physics present in OPVs, rigorous and reliable measurement techniques for charge transport and charge recombination are needed to construct improved physical models that can guide materials development and discovery. Here, we develop a new technique called impedance-photocurrent device analysis (IPDA) to quantitatively characterize the competition between charge extraction and charge recombination under steady state operational conditions. The measurements are performed on actual lab scale solar cells, have mild equipment requirements, and can be integrated into normal device fabrication and testing workflows. We perform IPDA tests on a broad set of devices with varying polymer:fullerene blend chemistry and processing conditions. Results from the IPDA technique exhibit significantly improved reliability and self-consistency compared to the open-circuit voltage decay technique (OCVD). Inaccessible to most other common measurement techniques, IPDA measurements also reveal a significant negative electric field dependence of the bimolecular recombination coefficient in high fill factor devices, indicating that the most common measurement techniques may overestimate the value that is most relevant for describing the device performance. Future work utilizing IPDA to build structure-property relationships for bimolecular recombination will lead to enhanced design rules for creating efficient OPVs that are suitable for commercialization.

I. INTRODUCTION

Organic photovoltaics (OPVs) have generated great interest over the last two decades for their potential as a unique renewable energy generation technology, and their performance continues to improve with a large diversity of materials that can now reach over 10% power conversion efficiency (PCE) and the best certified PCE now at almost 15%.[1,2] To compete with established inorganic semiconductor-based technology and other emerging technologies, such as perovskite and quantum dot solar cells, the power conversion efficiency (PCE) must continue to improve. Tremendous progress has been achieved in understanding how to tune chemical structures to modulate the electronic energy levels and thereby increase the short-circuit current (J_{sc}) and the open-circuit voltage (V_{oc}) largely following the Scharber model.[3] However, developing design rules to maximize the fill factor (FF) has been and continues to be a much more difficult task, and there are still major fundamental questions that make materials discovery and development a slow, expensive, and challenging process.

In most optimized devices, it is now well-established that the fill factor is primarily dictated by a competition between charge carrier extraction and bimolecular charge recombination.[4–6] As a result, bimolecular recombination is the dominant loss process that limits the PCE in the best bulk heterojunction (BHJ) OPVs.[7] This loss process occurs when an electron and a hole, which are not generated from the same absorbed photon, meet and recombine within the active layer. Under conditions most relevant for OPVs, where the photogenerated charge carrier density is greater than the intrinsic density, the recombination process follows is a simple second-order reaction,

$$R_{\mathrm{br}} = -\frac{dn}{dt} = k_{\mathrm{br}} n^2, \qquad (1)$$

where k_{br} is the bimolecular recombination coefficient and n is the total charge carrier density under illumination.

Many studies have also shown that bimolecular recombination losses can be mitigated by having a high charge carrier mobility.[8] A comprehensive study by Bartesaghi *et al.*, combined drift-diffusion simulations and advanced experimental device characterization methods to show

that the fill factor is dictated by a newly derived quantitative figure of merit referred to here as the competition factor,

$$\theta = \frac{k_{\mathrm{br}} G L^4}{\mu_{\mathrm{e}} \mu_{\mathrm{h}} V_{\mathrm{int}}^2}, \qquad (2)$$

where G is the charge generation rate, L is the active layer thickness, μ_e and μ_h are the electron and hole mobilities, respectively, and V_{int} is the internal voltage in the device at maximum power.[5] To obtain optimized devices with a high fill factor, θ must be as small as possible, and while a high fill factor can often be achieved by reducing the active layer thickness, thicker layers absorb more light and generate more photocurrent. Instead, given equal electron and hole mobilities, one would like to minimize k_{br}/μ^2.

From a commercial application perspective, a lower recombination rate and higher mobility allows devices to have a thicker active layer while maintaining a good fill factor, which makes it easier to manufacture high performance devices via roll-to-roll printing methods. However, rational design principles for materials which have both a high mobility and a low bimolecular recombination rate are missing. Understanding the detailed factors, including chemical structure, donor-acceptor pairing, and morphology, that dictate the eventual charge carrier mobility and recombination rate in real devices are some of the most critical fundamental problems in the OPV research field.

It is then imperative to understand the factors that control the magnitude of the bimolecular recombination coefficient. As a reference point, the Langevin model describes the upper limit of the recombination coefficient such that

$$k_{\mathrm{L}} = \frac{q}{\epsilon \epsilon_0} (\mu_{\mathrm{e}} + \mu_{\mathrm{h}}), \qquad (3)$$

where q is the elementary charge constant, ϵ is the relative permittivity of the material, and ϵ_0 is the vacuum permittivity constant.[9] This model assumes that the recombination process is encounter-limited such that electrons and holes recombine immediately upon meeting and that the process occurs in a homogeneous medium. However, in BHJ OPVs, electron donor and acceptor materials phase separate to form a nano-structured domain morphology and experimentally, BHJ films have been found to show very complex recombination behavior that frequently deviates from the Langevin model.[7] Most importantly, in some blends, the recombination rate has been found to be significantly less than what is predicted by the Langevin model, and as a result, studies often determine the Langevin reduction factor (ζ), where

$$\zeta = \frac{k_{br}}{k_{\mathrm{L}}}, \qquad (4)$$

to characterize the recombination behavior, with measured values ranging from 1×10^{-4} to 1.[7] While a major

reduction was originally proposed to be due to the phase separated BHJ structure,[10] even blends with very similar morphology can have dramatically different recombination rates,[11] and simulations on model morphologies have shown that phase separated structures only cause a minor reduction.[12–14] The most prominent explanation for reduced recombination is that in some blends the recombination process is not encounter-limited but is instead reaction-limited, where charge carriers can meet at the donor-acceptor interface and then re-dissociate to form free charge carriers again.[14–20] However, further detailed studies are needed to determine which factors promote this process.

One of the key challenges in understanding and addressing this problem is a limitation in our ability to accurately and quantitatively measure the most relevant materials and device properties. Studies reporting recombination coefficients and charge carrier mobilities almost never include uncertainty estimates and measured values can vary by orders of magnitude depending on the measurement technique used and how the analysis is performed. For example, Clarke et al. have shown that different bimolecular recombination characterization techniques can give significantly different results, even when measured on the same set of samples by the same research group. Furthermore, Kiermasch et al. have recently shown that results from one of the most common types of technique, transient photovoltage, may often times be invalid.[22] Adding in sample variability and user error, one might be very hesitant to trust the quantitative accuracy of bimolecular recombination coefficient measurements reported in the literature. However, even when measurements are done correctly, most recombination characterization is done using transient measurement techniques that measure the decay of the charge carriers in a device under open-circuit conditions. These include transient photovoltage (TPV) based techniques, pump-probe transient absorption spectroscopy, and most charge extraction (CE) techniques (photo-CELIV, OTRACE, TDCF, BACE, etc.). While these techniques have provided great insight into the time dependence[11,23–27] and charge carrier density dependence[28–35] of the recombination coefficient, it can be difficult to determine which value is relevant for real devices under maximum power operating conditions.

If one measures the charge carrier density in the device at maximum power, one can interpolate a transient measurement to find the value of the recombination coefficient at the correct charge carrier density, but if the value is time and/or electric-field dependent, it is not possible to accurately determine the value relevant to the fill factor using these techniques. While Albrecht et al. have shown that the time delayed collection field (TDCF) method can be used to measure the bias dependence of the recombination coefficient, the extracted value will only be accurate if there is no time dependence. Overall, very few studies have determined how much the recombination coefficient changes between open-circuit

and maximum power conditions, so it is difficult to conclude how much this simplification may affect the previously reported results.

Similar issues are also present with characterizing the charge carrier mobility, where different techniques that measure at different timescales, charge carrier densities, and operating conditions can yield very different results.[23,37,38] Even using the most common space-charge-limited current technique to measure different materials and samples, Blakesley *et al.* has shown that variations in how different users measure and analyze their data can result in orders of magnitude difference in the final determined charge carrier mobility.[39] Combining separate measurements of the recombination coefficient and the mobility to calculate the Langevin reduction factor (ζ) and the competition factor (θ) only further increases the potential for inaccurate results depending on which techniques are used to measure each parameter. With these issues in mind, it is perhaps not a surprise that the experimentally determined θ values used by Bartesaghi *et al.* to demonstrate the validity of their model have apparent uncertainties of about 1 order of magnitude.[5] A broader collection of data from throughout the published literature would likely be scattered by several orders of magnitude.

Given these issues, there is a strong need for the development of well tested techniques that can provide accurate and reliable characterization of the bimolecular recombination kinetics and the charge carrier mobility that can then be used to construct meaningful structure-property relationships. To fully understand how the competition between charge extraction and recombination impacts the performance of real OPV devices, one must measure these characteristics on actual devices operating under 1 sun illumination and at maximum power conditions. To achieve this goal, we develop here a novel steady state technique called impedance-photocurrent device analysis (IPDA) and compare the results with a more traditional transient photovoltage technique called open-circuit voltage decay (OCVD). To broadly test and compare the two techniques, a wide range of polymer:fullerene BHJ OPVs with varying donor molecular structure, processing conditions, and active layer thicknesses are investigated.

II. THEORY AND METHODS

To illustrate the methods and data analysis procedures for the IPDA technique, we highlight the data measured on a 8.4% power conversion efficiency PTB7-Th:PC$_{71}$BM device (PTB7-Th #2). For fabrication details about this device and all other devices measured in this study, please refer to the Experimental section and the Supplementary Information.[40] In addition, for equation derivations and details about the fitting and analysis procedures used in this section, see the Supplementary Information.[40]

A. Measuring the Steady State Bimolecular Recombination Kinetics and Mobility

To determine the recombination coefficient under steady state, operational conditions, the overall generated current density (J) at a given applied bias (V) can be split into two components,

$$J(V) = J_{\mathrm{G}}(V) - J_{\mathrm{br}}(V), \qquad (5)$$

where $J_{\mathrm{G}}(V)$ is the effective generation current and $J_{\mathrm{br}}(V)$ is the bimolecular recombination current. By measuring and analyzing the photocurrent curves in the saturation regime, one can determine the generation current density at any applied bias, as shown in Fig. 1. Also shown is the automatically detected onset of the saturation regime (V_{sat}) for each photocurrent measurement.
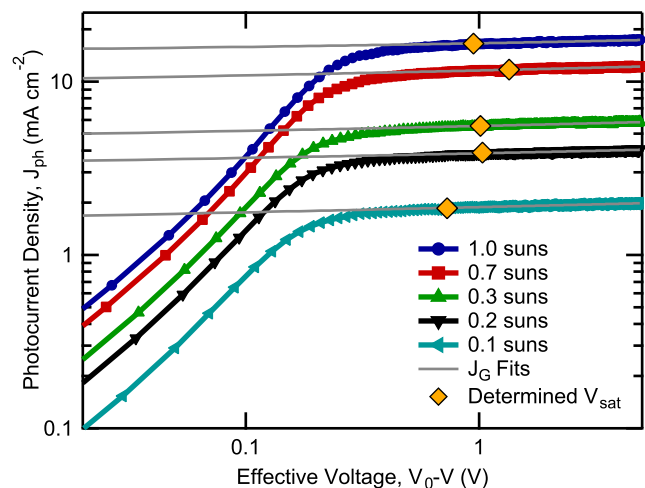

FIG. 1. Photocurrent curves for the device PTB7-Th #2 under different illumination intensities with power law fits to the saturation regime used to determine the effective generation current J_{G}.

This information can then used to calculate the complex bimolecular recombination coefficient,

$$k_{\mathrm{br}}(n, V) = \frac{J_{\mathrm{G}}(V) - J(V)}{qLn(V)^2}, \qquad (6)$$

where $n(V)$ is the charge carrier density in the device at the specified applied bias. To complete this calculation, an accurate measurement of $n(V)$ is needed.

To determine the effective mobility of the charge carriers in the working solar cell under various operational conditions, we expand on the method developed by Albrecht *et al.*.[41] The current density produced by a solar cell is dominated by the drift and diffusion current of electrons and holes traveling though the active layer, and at steady state, the electron and hole current densities must be equal. Assuming equal densities of electrons

and holes ($n = p$) and approximately equal charge carrier mobilities ($\mu_{\text{eff}} = \mu_{\text{e}} \approx \mu_{\text{h}}$),

$$\mu_{\text{eff}}(n, V) = \frac{J(V)L}{2qn(V)[V_{\text{oc}} - V]}. \tag{7}$$

Here again, a measurement of $n(V)$ is needed to complete the calculation.

Altogether, with highly accurate measurements of $n(V)$ in the range from short-circuit to open-circuit under various illumination intensities, one can determine the charge carrier density dependence and the electric field dependence of both the bimolecular recombination coefficient and the effective mobility in the operational range of the device.

B. Measuring the Charge Carrier Density with Impedance Spectroscopy

Two main types of techniques have been commonly used to determine the charge carrier density in OPVs under various operating conditions: charge extraction techniques and impedance spectroscopy. Here, we focus on developing a method using impedance spectroscopy, but we refer readers to several studies that have used charge extraction-based methods.[32,41] Both techniques can give the same information about the charge carrier density, but impedance spectroscopy has the advantage in that it can also be used to extract additional relevant information about the device such as the dielectric constant of the active layer. The experimental setup is also significantly simpler, only requiring a tunable steady state light source, a source measure unit, and an impedance analyzer.

Impedance spectroscopy has been a powerful tool for studying transport and recombination in OPVs, as well as in dye-sensitized and quantum dot solar cells.[42] To determined the charge carrier density, this technique requires the measurement of the chemical capacitance (C_μ) due to the charge carriers in the active layer as a function of the internal voltage. This relationship must then be integrated to determine the charge carrier density. Simply integrating from zero bias to open-circuit voltage has been often used to estimate the charge carrier density in OPVs under open-circuit conditions.[43,44] However, this method is not completely accurate because it assumes that the charge carrier density at short-circuit is zero. Basham *et al.* improved on this method by including an estimate of the charge carrier density at zero bias.[45] However, an even more accurate method was developed by Proctor *et al.* by determining the charge carrier density at a chosen point in the reverse bias saturation regime (n_{sat}),[46]

$$n(V) = n_{\text{sat}}(V_{\text{sat}}) + \frac{1}{qAL} \int_{V_{\text{sat}}}^{V_{\text{cor}}} C_\mu(V) dV_{\text{cor}} \tag{8}$$

where

$$n_{\text{sat}}(V_{\text{sat}}) = \frac{1}{qAL} C_\mu(V_{\text{sat}}) \left[V_0 - V_{\text{sat}} \right], \tag{9}$$

V_{sat} is the chosen point in saturation regime at which to perform the analysis, A is the device area, and V_0 is the voltage at which the photocurrent equals zero. V_{cor} is the corrected voltage drop across the active layer, which accounts for the voltage drop due to the series resistance of the circuit,

$$V_{\text{cor}} = V - J(V)AR_{\text{s}} \tag{10}$$

where R_s is the DC series resistance extracted from the dark *J-V* curve in forward bias regime where the current is resistance limited. This method allows the determination of the charge carrier density over a wide range from reverse bias to open-circuit conditions and has since been used in several studies to understand recombination in OPVs.[47–49]

In the majority of OPV impedance studies, the measurements have been analyzed using equivalent circuit modeling. Different equivalent circuits are often needed to fit the impedance response of OPVs. In some cases a simple RC circuit is sufficient,[46,48] but in other cases more complex circuits are needed, including constant phase element circuit[44,47] or a transmission line model.[50] Using equivalent circuit fitting must be done with great caution because the choice of the equivalent circuit can have an impact on the results, and different materials can require a different circuit model.

As a more universal method of analysis, Brus *et al.* proposed that calculation and analysis of the capacitance spectrum provides a model-free technique that can be used on any material.[49] Brus *et al.* determined the chemical capacitance at an analysis frequency of 10,000 Hz to estimate the density of free charge carriers. However, we are interested here in calculating the total charge carrier density. This requires the determination of the low frequency chemical capacitance plateau value, and here, we measure the device capacitance at a low frequency of 1000 Hz, where almost all charge carriers can contribute to the capacitive response. The chemical capacitance of the charge carriers is calculated,

$$C_\mu(V) = C_{\text{tot}}(V) - C_{\text{d}}, \tag{11}$$

where $C_{\text{tot}}(V)$ is the total capacitance of the solar cell under illumination measured at the target frequency as a function of the applied bias and C_{d} is the capacitance measured at the target frequency of the depleted device in the dark under reverse bias conditions. In previous studies,[46,48] the geometric capacitance (C_{g}) was subtracted from the total capacitance to calculate the chemical capacitance. In simple cases $C_{\text{d}} = C_{\text{g}}$, and the methods are equivalent. However, in cases where the depleted device exhibits a low frequency capacitive response due to ion motion or other slow molecular dipole rearrangements that cause dielectric relaxation,[51] this additional capacitance will be incorrectly assigned to charge

carriers, and the charge carrier density will be overestimated unless this additional capacitive contribution is subtracted from the total capacitance. As a result, subtracting C_d from the total capacitance should give a more accurate determination of the chemical capacitance due to the charge carriers. Here, we measure C_d as a function of frequency at $V = -4$ or -5 V. Figure 2(top) shows the final chemical capacitance as a function of the applied bias at various illumination intensities for the PTB7-Th #2 device.
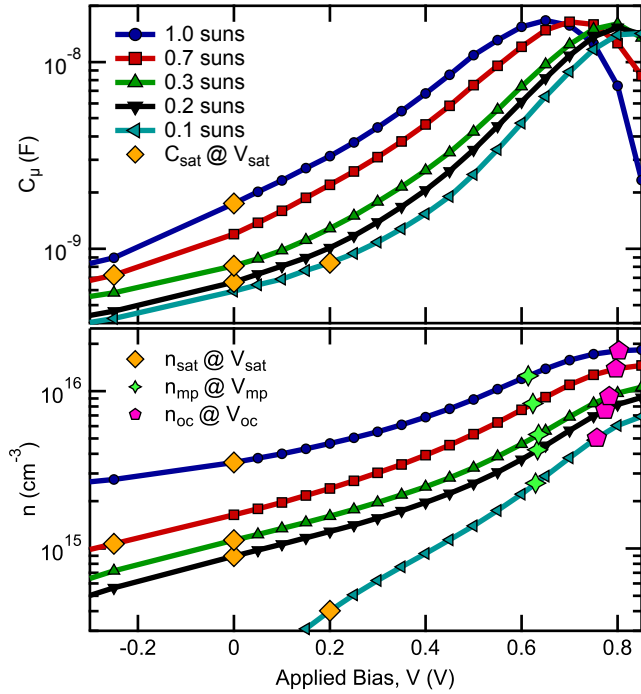

FIG. 2. Calculated chemical capacitance (top) and charge carrier density (bottom) curves for the PTB7-Th #2 device under different illumination intensities.

Nevertheless, the measurement of the geometric capacitance at high frequency (1 MHz) is still used to determine the dielectric constant of the active layer. With this measurement of the geometric capacitance, the effective

dielectric constant of the active layer blend is then calculated,

$$\epsilon = \frac{C_g L}{\epsilon_0 A}. \tag{12}$$

While the dielectric constant does not change much between many of the most common organic semiconductors used in OPVs, including those tested here, this measurement allows a more accurate calculation of the Langevin reduction factor that will account for possible changes in the dielectric constant of the active layer, instead of simply estimating the value at 3.5 or 4 as is often done in many other studies. Researchers developing new materials with a higher dielectric constant and investigating its effect on charge recombination could make particular use of this feature.[27,48,52,53]

We now reassess the derivation for the equation used to calculate the saturation charge carrier density (n_{sat}) shown in Eqn. 9. The original equation was derived under the assumption that the charge generation rate (G) and the effective mobility (μ_{eff}) are independent of the applied bias. However, if G and μ_{eff} are not independent of the the applied bias, then this equation will not be strictly valid. In a number of OPV blends, the charge carrier generation yield and the mobility can depend on the electric field or charge carrier density in the device, and a more detailed derivation of n_{sat} could take these effects into account.

The field dependence of the generation rate will appear as a slope in the photocurrent at large effective voltages. However, even in blends that do not have field-dependent generation of free charge carriers, the photocurrent may not saturate due to recombination of photo-generated charge carriers with injected charge carriers from the electrodes. Like geminate recombination, this type of recombination is also a first-order process and can be field-dependent.[54,55] Both field-dependent charge generation and field-dependent surface recombination with injected charges can then be combined to give the final field-dependent effective generation rate, $G(V)$, that determines the bias-dependence of the saturation current.

With these effects accounted for, n_{sat} has a more complex but complete form,

$$n_{sat}(V_{sat}) = \frac{C_\mu(V_{sat})}{qAL} \left[\frac{1}{V_{oc} - V_{sat}} + \frac{1}{J_G(V_{sat})} \frac{dJ_G(V_{sat})}{dV} - \frac{1}{\mu_{eff}(V_{sat})} \frac{d\mu_{eff}(V_{sat})}{dV} \right]^{-1} \tag{13}$$

With this final form, all values can be determined from the impedance measurements and simple J-V measurements except for the electric field dependence of the charge carrier mobility.

An accurate calculation of $n(V)$ requires a determination of $d\mu_{eff}/dV$ at $V = V_{sat}$. However, we also need to know $n(V)$ before we can calculate the bias dependence

of the mobility. As a result, the system is described by a series of nonlinear differential equations, and this system of equations can be solved numerically. This is done by first assuming $d\mu_{eff}(V_{sat})/dV = 0$ and calculating $n(V)$ using Eqns. 8 and 13. Then, $\mu_{eff}(V)$ is calculated using Eqn. 7, and the numerical derivative is calculated to update the value of $d\mu_{eff}(V_{sat})/dV$. This process is repeated

with the updated value for $d\mu_{\mathrm{eff}}(V_{\mathrm{sat}})/dV$, and multiple iterations are performed until n_{sat} converges.

Using the final n_{sat} value, $n(V)$ is calculated using Eqn. 8, as shown in Fig. 2(bottom) for the PTB7-Th #2 device. The process is repeated for measurements at different light intensities resulting in a series of $n(V)$ curves that are then interpolated to determine specific values of interest, such as the charge carrier density at the maximum power point (n_{mp}) or at open-circuit (n_{oc}) under various illumination intensities. Then using these $n(V)$ curves, the steady state bimolecular recombination coefficient and the effective charge carrier mobility under operating conditions can be determined using Eqns. 6 and 7, as shown in Fig. 3 for the PTB7-Th #2 device. Here again, specific values of interest can be determined such as the performance at maximum power and open-circuit conditions. However, the effective mobility cannot be explicitly determined at open-circuit because there is not current flowing at open-circuit, but one could extrapolate the measured values to open-circuit if desired.
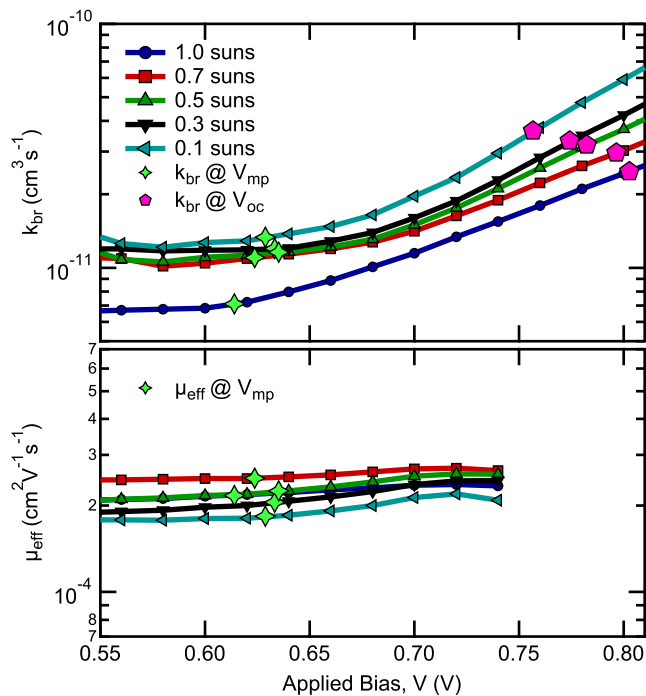

FIG. 3. Final calculated bimolecular recombination coefficient (top) and effective charge carrier mobility (bottom) as a function of applied bias for the PTB7-Th #2 device under different illumination intensities.

C. Measuring Bimolecular Charge Recombination with the Open-Circuit Voltage Decay Technique

As a comparison point, we also perform recombination measurements using the open-circuit voltage decay (OCVD) technique, which has been used in a number of previous studies to characterize the recombination kinet-

ics in OPVs.[22,56–61] In this measurement, the device is held under illumination at open-circuit conditions until steady state is reached. Then the light is quickly turned off, and the open-circuit voltage of the device is measured over time. By keeping the device at open-circuit for the entire duration of the experiment, there is no net current flowing in the device, and the photovoltage created by the splitting of the quasi Fermi levels due to the charge carriers inside the active layer is assumed to only be dissipated through the bimolecular charge recombination processes. All devices tested and analyzed here have a negligible contribution from the Shockley-Read-Hall trap-assisted recombination mechanism under the illumination intensities (I) of interest in this study ($>$ 0.1 suns), as evidenced by intensity dependent V_{oc} measurements in which linear fits to V_{oc} vs $\ln(I)$ plots yield slopes less than 1.1 kT/q.[62,63]

In an OCVD measurement, one could simply calculate the voltage lifetime. However, the voltage lifetime alone provides limited information, and what is really desired is a measurement of the charge carrier density transient, so that a more detailed analysis of the recombination kinetics can be performed. In OPVs, the relationship between the measured open-circuit voltage (V_{oc}) and the charge carrier density has been shown to depend on the charge transfer state energy (E_{CT}) and further modified depending on the functional form and magnitude of the density of states (DOS).[48,64,65] For both Gaussian and exponential DOS models, assuming $n = p$, the open-circuit voltage can be generally expressed,

$$V_{\mathrm{oc}} = E_0 + \frac{m_{\mathrm{d}} k_{\mathrm{B}} T}{q} \ln n_{\mathrm{oc}}^2. \tag{14}$$

where E_0 is a fit parameter, m_{d} is the disorder prefactor, k_{B} is the Boltzmann constant, and T is the temperature. Using this relationship, we fit Eqn. 14 to a series of measurements of V_{oc} and n_{oc} at different light intensities and then use it as a master curve for converting open-circuit voltage transient measurements into a charge carrier density transients, as shown in Fig. 4 for the PTB7-Th #2 device.

In addition to reduced recombination, super-second order recombination kinetics have often been observed in OPVs.[7] In most cases, the recombination mechanism itself is still second-order, but there is assumed to be a charge carrier density dependent rate coefficient. Following the commonly used method introduced by Shuttle et al.,[28] the rate equation can be more generally expressed,

$$R_{\mathrm{br}} = -\frac{dn}{dt} = k_{\mathrm{br}}(n)n^2, \tag{15}$$

where the charge carrier density dependence of the rate coefficient is often expressed using a simple power-law,

$$k_{\mathrm{br}}(n) = k_0 n^{\lambda-1}, \tag{16}$$

in which k_0 and λ are fit parameters. Taking this into account, the charge carrier density transients can be fit
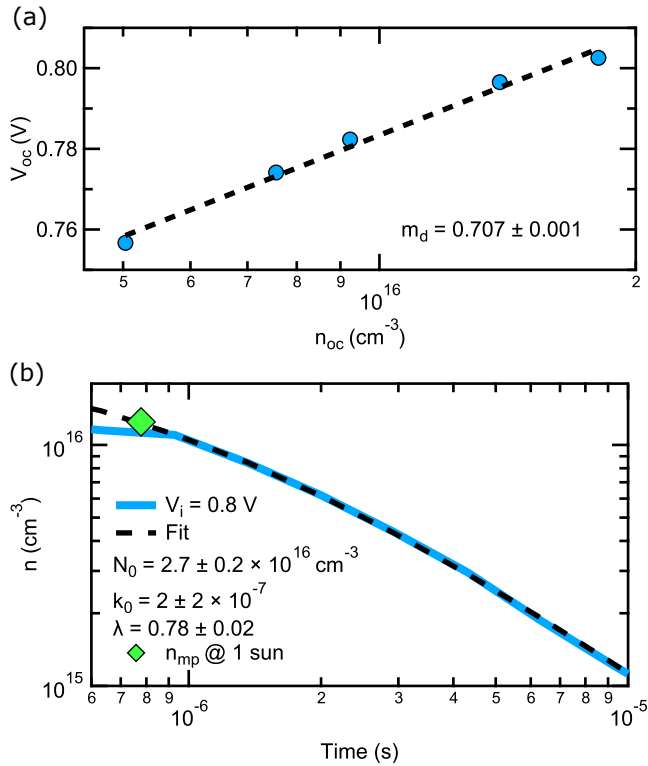
FIG. 4. (a) Eqn. 14 fit to V_{oc} vs n_{oc} data and (b) Eqn. 17 fit to charge carrier density transients for the PTB7-Th #2 device under different illumination intensities.

using the integrated form of Eqn. 16,

$$n = n_0 \left[1 + \lambda k_0 t n_0^\lambda \right]^{-1/\lambda}, \qquad (17)$$

where n_0 is the initial charge carrier density at time equals zero, and t is the time. Fitting this equation to charge carrier density transients allows one to extract the fit parameters k_0 and λ, and then determine the recombination order ($\lambda+1$) and calculate $k_{br}(n)$ using Eqn. 16.

III. RESULTS AND DISCUSSION

To broadly test the IPDA technique and determine general trends in the device characteristics and performance, a wide range of polymer:fullerene blends was tested. This includes the well-characterized reference blends P3HT:PC$_{61}$BM[66,67] and PTB7:PC$_{71}$BM.[68,69] In addition, we also selected several newer and higher performing blends, including PTB7-Th:PC$_{71}$BM[70] and PPDT2FBT:PC$_{71}$BM,[71,72] and performed further analysis on the previously measured PIPCP:PC$_{61}$BM blend.[61,73] For each polymer:fullerene blend system, representative high quality devices were selected from batches of >10 devices for running the full IPDA and OCVD measurement protocol. From the total dataset, we take a detailed look at 8 exemplary devices with distinct blend chemistry or different film fabrication conditions. For the P3HT:PC$_{61}$BM,

PTB7:PC$_{71}$BM, and PTB7-Th:PC$_{71}$BM blends, we fabricated and tested an un-optimized, as-cast film as well as an optimized blend using annealing or solvent additives. P3HT:PC$_{61}$BM films were cast from 1,2-dichlorobenzene (DCB); PTB7:PC$_{71}$BM films were cast from chlorobenzene (CB) using the solvent additive diiodooctane (DIO); PTB7-Th:PC$_{71}$BM films were cast from CB using the solvent additive diphenyl ether (DPE); PPDT2FBT:PC$_{71}$BM films were also cast from CB using the DPE solvent additive; and PIPCP:PC$_{61}$BM films were cast from a solvent mixture of CB with chloroform (CF). General fabrication information for the 8 exemplary devices is shown in Table I with more details including chemical structures provided in the Supplementary Information.[40] The same measurement methods described above were applied to all devices.

A good starting point for comparing techniques is taking a more detailed look at two of the most well-characterized systems, annealed P3HT:PC$_{61}$BM[10,30,31,35,74,75] and PTB7:PC$_{71}$BM fabricated with DIO,[31,32,76–78] which have both been characterized by a number of the most common recombination measurement techniques by different research groups. Figure 5 shows measurements of the bimolecular recombination coefficient as a function of the charge carrier density as determined by several different transient techniques from the literature. In general agreement with these values, our measurements of device P3HT #2 and PTB7 #2 using OCVD shows a recombination coefficient that has almost no charge carrier density dependence and a value of approximately 2×10^{-12} cm^{3}s^{-1} for P3HT #2 and 3×10^{-11} cm^{3}s^{-1} for PTB7 #2 under open-circuit conditions.

While our OCVD results are close to that of several previously published studies, there is significant variability between different published studies up to almost 1 order of magnitude. Despite measuring approximately the same blend materials fabricated in a very similar way, these studies show significant variation in the recombination coefficient likely due to a combination of factors, including source materials batch variation, minor film fabrication differences, and measurement technique differences. Such variability often makes it difficult to compare results between studies. However, here we perform IPDA and OCVD measurements on the same device to help rule out sample variability concerns. The IPDA measurements on both the P3HT and PTB7 blends reveal a consistent decrease of almost 1 order of magnitude compared to OCVD when measuring the recombination coefficient at maximum power. This difference between the value of the recombination coefficient at open-circuit and maximum power in the optimized P3HT and PTB7 blends is even greater than observed for the PTB7-Th #2 device in Fig. 3. This demonstrates that in at least several cases, transient-based measurements of the recombination coefficient at open-circuit can significantly overestimate the value of the recombination coefficient that ultimately determines the fill factor.

TABLE I. General OPV Device Fabrication Data

| Device	Donor	Acceptor	Ratio(wt/wt)	Casting Solvent	Thermal Annealing	L(nm)
P3HT #1	P3HT	$PC_{61}BM$	4:3	DCB	none	135
P3HT #2	P3HT	$PC_{61}BM$	4:3	DCB	Slow dry, $150°$ C for 20 min	260
PTB7 #1	PTB7	$PC_{71}BM$	2:3	CB	none	90
PTB7 #2	PTB7	$PC_{71}BM$	2:3	CB + 3 vol% DIO	none	90
PTB7-Th #1	PTB7-Th	$PC_{71}BM$	2:3	CB	none	85
PTB7-Th #2	PTB7-Th	$PC_{71}BM$	2:3	CB + 3 vol% DPE	none	120
PPDT2FBT	PPDT2FBT	$PC_{71}BM$	2:3	CB + 3 vol% DPE	none	125
PIPCP	PIPCP	$PC_{61}BM$	1:2	3:2 CB:CF	none	110
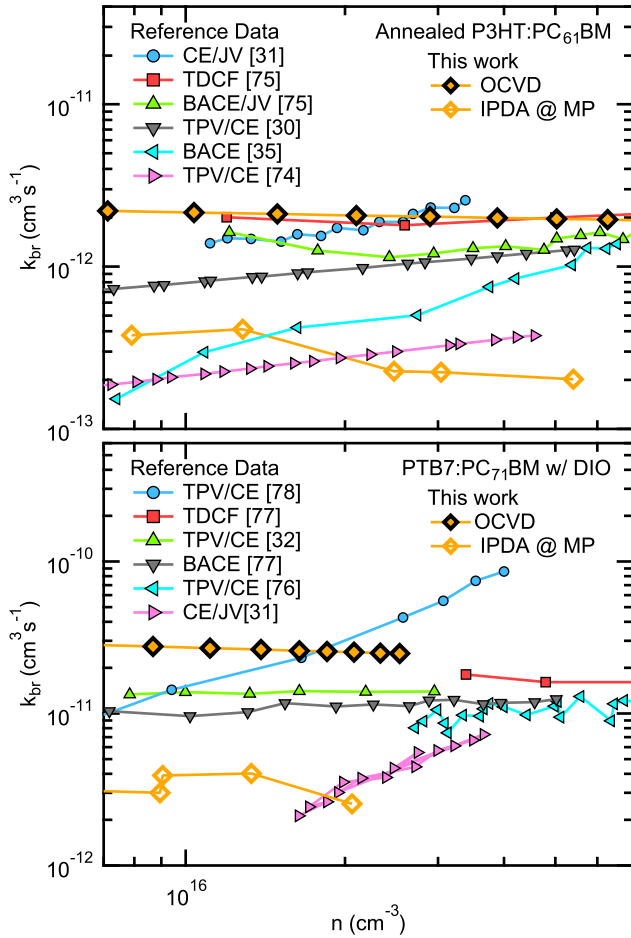
FIG. 5. Comparison of recombination coefficient measurements for (top) annealed P3HT:$PC_{61}BM$ blends and (bottom) PTB7:$PC_{71}BM$ blends fabricated with DIO solvent additive.

To look further into this difference, we compare the bimolecular recombination coefficients determined using each method for each of the 8 exemplary devices in Fig. 6. For the values derived from the OCVD measurement, k_{br} is determined at the charge carrier density at maximum power (n_{mp}) under 1 sun illumination. As a result, both the IPDA and OCVD derived measurements are at the same charge carrier density but at a different applied bias

condition. All devices except the PIPCP device show a significantly lower recombination coefficient from IPDA than from OCVD. However, it is not a simple offset either. There is a variable difference that evidently depends on the details of the materials and morphology, but a difference that can reach up to a 1 order of magnitude in several of the cases tested here. In addition, the difference between the two techniques appears to be greater for the optimized devices than the un-optimized devices. In addition to the inability of OCVD to account for a time and/or electric field dependent k_{br}, another possible contribution is that a lack of blocking layers can cause recombination with injected carriers to have a significant impact on the transient voltage decay.[79] Without a way to subtract this component, OCVD measurements may overestimate the true bimolecular recombination coefficient. In contrast, steady state IPDA measurements subtract any possible bias-dependent first order losses, such as recombination with injected charge carriers, when calculating the bimolecular recombination current.

To probe these differences further and help decide which technique yields measurements that are most consistent with the device performance, the competition factor (θ) is calculated using Eqn. 2. To do so, the generation rate is determined at maximum power from the photocurrent analysis, $G = J_G(V_{mp})/qL$. The product of the electron and hole mobility is replaced by μ_{eff}^2 determined from the IPDA technique, and $V_{int} = V_{oc} - V_{mp}$. Two variants of the competition factor are then calculated, θ_{IPDA}, where the k_{br} used is the value from IPDA, and θ_{OCVD}, where the k_{br} used is the value from OCVD. This analysis and calculation was done for the 8 exemplary and also for a number of additional replicate devices and devices with other fabrication variations. For more details about all of the devices shown here, see the Supplementary Information.[40] From this collection of 34 devices, those with significant field-dependent charge generation, including the as-cast P3HT:$PC_{61}BM$ devices and PTB7:$PC_{71}BM$ devices made without the DIO solvent additive, were removed from the dataset. Significant field-dependent charge generation reduces the fill factor, but this phenomenon is not included in the derivation of the Bartesaghi model. For the remaining 28 devices, Fig. 7 shows how the two differently calculated compe-
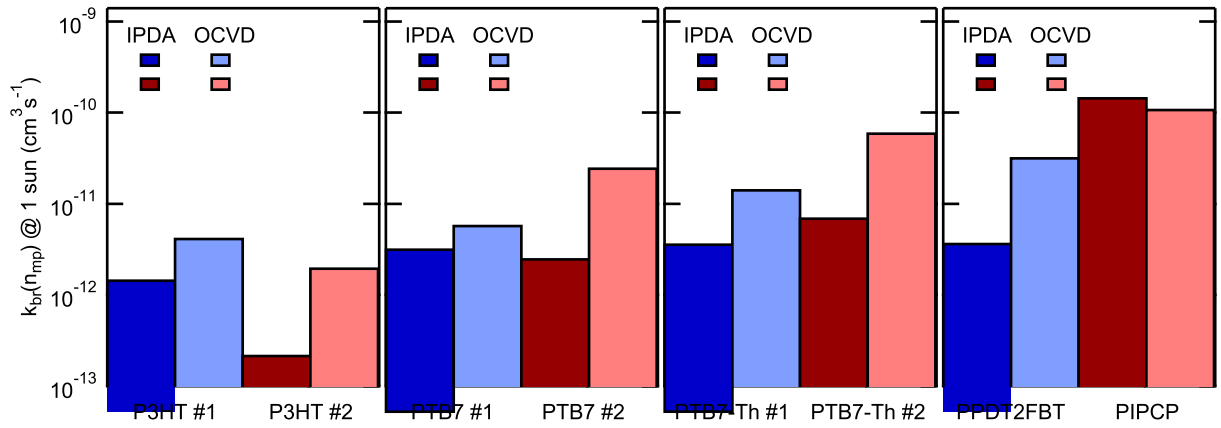
FIG. 6.   Comparison of bimolecular recombination coefficient values determined at n_{mp} under 1 sun illumination with the IPDA and OCVD techniques.
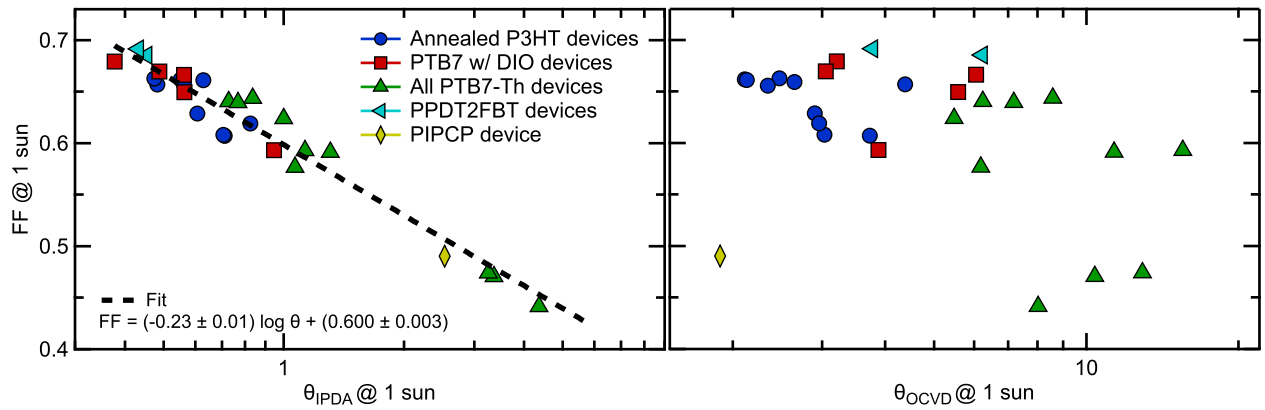

FIG. 7.   Comparison of the competition factor (θ) determined using k_{br} values at n_{mp} from the IPDA and OCVD techniques.

tition factors compare with the fill factor measured on the same device under 1 sun illumination. The results from the IPDA technique show a very clear correlation between the competition factor and FF as predicted previously, while the results from OCVD show no clear correlation. This provides further evidence supporting recent work by Kiermasch *et al.* indicating that transient photovoltage based techniques do not given reliable measurements of the bimolecular recombination kinetics in thin film solar cells.[22] Conversely, the IPDA technique gives results that are self-consistent between many different devices with different polymer:fullerene blend chemistries, processing conditions, and active layer thicknesses. Furthermore, the final calculated θ values have apparent uncertainties that are less than $\pm 25\%$, which is a major improvement over the dataset collected by Bartesaghi *et al.*.[5] In addition, the OCVD-derived θ_{OCVD} results are shifted to larger values, further indicating that OCVD overestimates k_{br} compared to the IPDA technique.

Analyzing IPDA competition factor results, we find that the fill factor is proportional to $\log(\theta_{\mathrm{IPDA}})$ over the parameter range tested here. Beyond the range tested here, the FF is expected to plateau at both the high end and the low end, thereby forming a inverted S shape

that can be fit by a sigmoid function.[80] However, over the range tested here, a simple linear model is sufficient. Further IPDA measurements at the extremes would be needed to test the functional relationship further, but a detailed functional analysis of the FF-θ relationship is beyond the scope of this study. In the future, more detailed model fitting could potentially be used to extract parameters that may provide further physical understanding of the transport and recombination behavior.

A more detailed look at the device characteristics determined for the 8 exemplary devices is shown in in Table II Most importantly, one can compare how the recombination coefficient and the effective mobility vary between the different devices. Perhaps the most striking observation is that the effective mobility of all of the optimized devices is very similar. Despite significant changes in donor molecular structure and other properties, the effective mobility of the blends only range between 1×10^{-4} and 3×10^{-4} cm^{2}V^{-1}s^{-1}. In stark contrast, the recombination coefficient between the same series of devices varies by over 2 orders of magnitude. This leads to an important point about where to focus future research efforts. While high mobility has certainly been shown to be important for creating high fill factor

TABLE II. IPDA 1 Sun Maximum Power Point Characterization Data

Device	$J_{sc}(mAcm^{-2})$	$V_{oc}(V)$	FF	PCE(%)	$n_{mp}(cm^{-3})$	$k_{br}(cm^3s^{-1})$	$\mu_{eff}(cm^2V^{-1}s^{-1})$	ζ	θ
P3HT #1	-3.8	0.63	0.61	1.4	2×10^{16}	2×10^{-12}	6×10^{-5}	2×10^{-2}	1
P3HT #2	-9.5	0.57	0.66	3.6	3×10^{16}	2×10^{-13}	2×10^{-4}	1×10^{-3}	0.5
PTB7 #1	-8.9	0.74	0.51	3.4	3×10^{16}	3×10^{-12}	3×10^{-5}	1×10^{-1}	3
PTB7 #2	-15.6	0.73	0.65	7.4	2×10^{16}	3×10^{-12}	1×10^{-4}	3×10^{-2}	0.6
PTB7-Th #1	-12.9	0.78	0.47	4.8	3×10^{16}	4×10^{-12}	4×10^{-5}	1×10^{-1}	3
PTB7-Th #2	-16.4	0.80	0.64	8.4	1×10^{16}	7×10^{-12}	2×10^{-4}	3×10^{-2}	0.7
PPDT2FBT	-11.1	0.76	0.69	5.8	1×10^{16}	4×10^{-12}	2×10^{-4}	1×10^{-2}	0.4
PIPCP	-15.0	0.90	0.49	6.6	6×10^{15}	7×10^{-11}	3×10^{-4}	2×10^{-1}	2

devices,[4,81] it may be difficult to significantly improve beyond 1×10^{-3} cm^{2}V^{-1}s^{-1} in disordered BHJ morphologies. Instead, perhaps a more concerted effort to develop materials with slow bimolecular recombination would be more fruitful given that its value can vary so dramatically even between already highly optimized blends. As shown previously, phase separation alone is not sufficient to produce highly reduced recombination.[11–14] Instead, charge carrier re-dissociation is proposed to largely dictate the eventual bimolecular recombination rate.[14–20] However, design rules for creating blends with these properties are still lacking.

When comparing the un-optimized and optimized P3HT:PC$_{61}$BM, PTB7:PC$_{71}$BM, and PTB7-Th:PC$_{71}$BM blends an interesting feature is observed. While the use of annealing or solvent additives in the optimized blends significantly increases the mobility relative to the un-optimized devices, optimizing the morphology decreases the recombination coefficient only in the P3HT:PC$_{61}$BM blend. In the PTB7:PC$_{71}$BM blend, the recombination coefficient is largely unchanged by the solvent additive. Previous work by Kniepert *et al.* measured a decrease in k_{br} by a factor 2-3 when using DIO with PTB7:PC$_{71}$BM blends, but the precise reason for this discrepancy cannot be elucidated here. Given the typically large variation seen between different samples and measurement techniques, as shown in Fig. 5, a factor of 2-3 difference may not significant in many cases. Finally, in PTB7-Th:PC$_{71}$BM blends, using solvent additives actually slightly increases the recombination coefficient. Further understanding of how morphology optimization procedures affect the recombination coefficient is needed to try and identify ways to both increase the mobility and decrease the recombination coefficient as is observed in the P3HT:PC$_{61}$BM blend.

However, based on previous detailed morphological studies, several observations can be made. Annealing of P3HT:PC$_{61}$BM blends has been shown to cause enhanced phase separation that is driven by crystallization of the P3HT phase, forming a final 3-phase morphology with high purity polymer and fullerene domains and a more disordered mixed phase inbetween.[82] Formation of an interfacial mixed phase has been shown to cause energy cascades that can promote charge separation,[83–85] and these energy cascades could also potentially inhibit bimolecular charge recombination. In contrast, with PTB7:PC$_{71}$BM blends, previous studies have shown that the use of DIO prevents over-ripening of the fullerene domains to create an optimal nanoscale phase separated morphology.[68] However, unlike P3HT:PC$_{61}$BM, only 2-phases are found, and the optimized blend contains PTB7-rich donor phases with significant fullerene content.[86] In the PIPCP:PC$_{61}$BM blend, which has the highest recombination rate, a well-mixed morphology was identified without the formation of any pure or enriched phases.[61]

These results appear at least qualitatively consistent with recent work that has emphasized the role of phase purity in reducing the bimolecular recombination rate and increasing the fill factor.[87–90] However, it is still unclear whether a 2-pure phase or 3-phase morphology is better and if the molecular scale donor-acceptor interactions and orientations that determine the charge transfer state lifetime are also important. The IPDA measurement technique developed here is well-suited to play a significant role in concert with detailed morphology characterization techniques to elucidate these mechanisms further.

Beyond the basic characterization of the device behavior at 1 sun illumination conditions, a series of illumination intensity dependent measurements also allows one to determine both the charge carrier density dependence and the electric field dependence of the bimolecular recombination coefficient, the effective charge carrier mobility, and the Langevin reduction factor. Characterizing and understanding these dependencies can help shed light on their physical origins. Different combinations of illumination intensity and applied bias can result in the same value of the charge carrier density, so one can then fix the charge carrier density and determine the bias (electric field) dependence of each parameter over the measured range. Here, choosing a relatively low charge carrier density allows interpolation over a large enough range of electric field strengths to see meaningful trends. Figure 8 shows the field dependence of each parameter for all 8 exemplary devices. Again, here we see the dramatic difference in recombination coefficient between the various polymer:fullerene blends, and all of the optimized

blends, except for PIPCP:PC$_{61}$BM, show a negative electric field dependence.
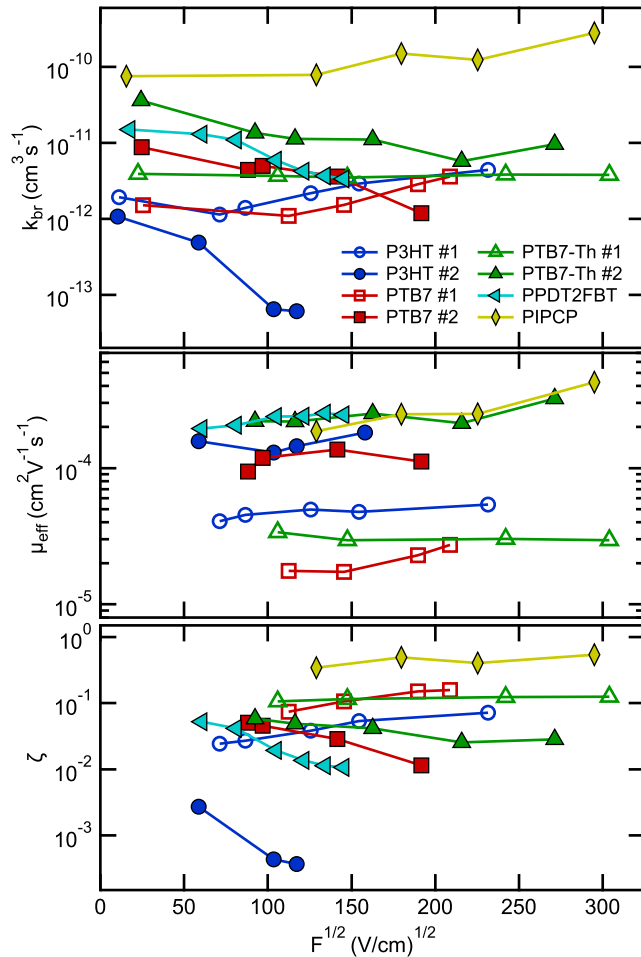

FIG. 8. The electric field dependence of the bimolecular recombination coefficient (top), effective mobility (middle), and Langevin reduction factor (bottom) for all 8 devices at $n = n_{oc}(I = 0.1$ sun$)$, which is the charge carrier density of the device at open-circuit under 0.1 sun illumination.

In agreement with our observed trends, Albrecht *et al.* have shown using TDCF measurements that the recombination coefficient in an optimized PCPDTBT:PC$_{71}$BM blend decreases by approximately a factor of 2 when going from open-circuit to maximum power.[36] They attributed this behavior to a mobility with a negative field dependence, finding that the reduction factor is essentially independent of the electric field. In contrast, our results for optimized P3HT, PTB7, PTB7-Th, and PPDT2FBT devices all show essentially field independent mobility such that the field dependence of the recombination coefficient carries though to give a field dependent reduction factor. Our observation of largely field independent mobility in these devices is consistent with BHJ morphologies that have relatively direct charge transport pathways (mild tortuosity).[91] A highly negative field dependence that would indicate a morphology

with undesirably convoluted charge transport pathways (high tortuosity) is not observed for these materials.

Interestingly, there also appears to be a correlation between the magnitude of the reduction factor and the electric field dependence, with the most reduced recombination in the P3HT #2 device also having the strongest field dependence. A negative field dependence of the bimolecular recombination coefficient in a neat disordered semiconductor has been shown before theoretically,[92] and a field-activated polaron pair re-dissociation at the donor-acceptor interface could potentially explain the negative field dependence. However, further studies are needed to quantify and understand this phenomenon, and IPDA measurements would be uniquely able to probe this further. For many years, annealed P3HT:PCBM blends have been known to have the lowest recombination rates of any other blend, and it is one of the key reasons why it can achieve good performance even with a thick active layer. Recently, Gasparini *et al.* have determined an even lower recombination rate in the non-fullerene P3HT:IDTBR blend.[93] Further understanding of how P3HT is able to achieve this behavior, identifying additional materials with extremely slow recombination, and accurately quantifying the transport and recombination parameters represents a major opportunity for high impact OPV research going forward.

IV.　CONCLUSIONS

In order to increase the accuracy and reliability of charge transport and recombination measurements for OPVs, we have developed the impedance-photocurrent device analysis (IPDA) technique for measuring real devices under standard, steady state operating conditions, and we apply the technique to a wide range of polymer:fullerene blends prepared with various fabrication conditions. As a comparison point, we also apply a more common transient photovoltage technique called open-circuit voltage decay (OCVD) to the same set of devices. We find that IPDA gives a much more reliable quantification of the recombination kinetics than the OCVD method, and that altogether, IPDA characterization of both charge transport and recombination correlates very well with the device fill factor when using the Bartesaghi model.[5] The IPDA measurement results compiled here on many different devices with a variety of blend chemistries, processing conditions, and active layer thicknesses represent one of the most self-consistent and comprehensive charge transport and recombination datasets available for OPVs. Our results also provide further supporting evidence that common transient photovoltage based techniques do not give reliable measurements of the bimolecular recombination kinetics in thin film solar cells, as shown recently by Kiermasch *et al.*.[22] Furthermore, we find that very often, the bimolecular recombination coefficient is significantly less at maximum power operating conditions than at open-circuit, even after correcting

for the charge carrier density dependence. As a result, even charge extraction based techniques that measure recombination at open-circuit may often overestimate the recombination coefficient. Further analysis reveals that most of the optimized devices tested here exhibit a recombination coefficient with a significant negative electric field dependence, which is not probed by most of the common recombination characterization techniques.

Overall, we find IPDA to be a powerful technique that will allow researchers to characterize the primary device properties that ultimately determine the fill factor in most high performance OPVs. The reliability and reduced measurement uncertainty afforded by the IPDA technique could allow researchers to identify and more rigorously study materials that can maintain a high fill factor with a thick active layer. Recently, an increasing number of fullerene and non-fullerene blends have been able to achieve a high fill factor in thick films,[72,89,94–99] so there is great opportunity for elucidating the physical mechanisms that drive this behavior. While we have only investigated polymer:fullerene blends in this study, there should be no reason that the technique cannot also be applied to the wide variety of small molecule:fullerene blends, non-fullerene acceptor blends, polymer-polymer blends, co-evaporated BHJ blends, and even ternary blends that all continue to be developed. As long as the blends have a BHJ architecture and meet the assumptions laid out in this study, IPDA should be equally applicable. Future work utilizing IPDA to build structure-property relationships for bimolecular recombination could lead to enhanced design rules for creating efficient OPVs that are suitable for commercialization.

IPDA could also play a role in increasing the rate of OPV materials discovery and optimization. In this vein, most work has been focused on using *ab initio* electronic structure methods to screen for appropriate chemical structures, largely based on their optical bandgap.[100–102] While this can be a useful method to narrow the search, *in silico* predictions of the fill factor are extremely difficult due the highly complex series of factors that determine its value, and such methods cannot currently capture processing and morphology effects. Recent work has highlighted the importance of the thermodynamic parameter χ on the fill factor and suggested higher throughput miscibility experiments could be used to accelerate materials discovery,[90] but knowing χ alone is not enough to accurately predict the fill factor nor the fabrication conditions required to reach a particular level of performance. Instead of replacing device experiments completely, reliable higher throughput experimental characterization techniques that can generate information-rich databases could enhance recent efforts to create predictive data-driven models using machine learning.[103] IPDA measurements are performed on actual lab scale solar cells, have mild equipment requirements, can be integrated into existing device fabrication and testing workflows, and yield a range of detailed metrics, thereby greatly increasing the scientific value of each experimental device fabricated. A starting example of such an information-rich dataset containing detailed starting materials properties, film fabrication details, and IPDA device characterization results is provided in the Supplementary Data file. Combining this approach with various materials screening efforts could be a promising strategy for significantly reducing trial-and-error approaches to OPV materials development.

V. EXPERIMENTAL

Device Fabrication: Glass substrates with 140 nm of indium tin oxide (ITO) from Naranjo Substrates were scrubbed with soapy DI water and sonicated in acetone and then isopropanol before being treated with O2 plasma. Then, a 40 nm PEDOT:PSS (Clevios P VP Al 4083) layer was spin coated at 2500 rpm and dried at 140° C in air for 20 min. Active layers were then deposited in a N2 glovebox using a spin coater. P3HT was used as received from Plextronics (Plexcore OS 2100). PTB7 and PTB7-Th were used as received from 1-Material. PPDT2FBT was synthesized as reported previously.[71,72] $PC_{61}BM$ and $PC_{71}BM$ were used as received from Nano-C. Top contacts consisting of approximately 15 nm of calcium and 100 nm of aluminum were thermally evaporated onto the active layer using an Angstrom Engineering Amod vacuum deposition system. PIPCP was synthesized using the previously reported method,[73] and measurements were performed on a previously fabricated and characterized device with an inverted architecture.[61] Layer thicknesses and device area were measured using an Ambios XP-100 stylus profilometer. Device area for all samples was approximately 0.2 cm^2, except for the $PIPCP:PC_{61}BM$ device that was only 0.06 cm^2.

Current-Voltage Measurements: Devices were tested in a N2 glovebox and illuminated without an aperture using a 100 mW cm^2 simulated AM1.5G light source from a Newport 66902 300 W XE arc lamp with an AM1.5 global filter. Lower illumination intensities were obtained using a Newport 5215 optical density filter wheel. The light source irradiance was calibrated using a standard monocrystalline silicon reference cell with a KG5 filter calibrated by the National Renewable Energy Laboratory. Measurements were performed using a Keithley 2602A source-measurement unit controlled by National Instruments LabView software.

OCVD Measurements: Devices were tested in a vacuum sample chamber and illuminated with a Cree XT-E high-power white LED on a Indus Star metal core printed circuit board for heat dissipation. The LED had a measured turnoff lifetime of $\approx$ 200 ns, which gives a measurement time resolution of 500 ns. The LED was powered by a power source connected to a high power transistor switch. The device was connected to a high impedance voltage follower, which allows the open-circuit voltage of the solar cell to be measured without allowing cur-

rent to flow through the circuit. The voltage output from the voltage follower was measured using a Tektronix TDS5032B digital oscilloscope. The LED switch and the oscilloscope were triggered using a square function from a Tektronix AFG320 function generator.

Impedance Measurements: Devices were measured using a Solartron 1260 impedance analyzer with an AC amplitude of 100 mV. Measurement scripts and instrument control was done using ZPlot software from Scribner Associates, Inc.

VI. CONFLICTS OF INTEREST

There are no conflicts of interest to declare.

VII. ACKNOWLEDGEMENTS

---

* heiber@mailaps.org
† quyen@chem.ucsb.edu

[1] X. Che, Y. Li, Y. Qu, and S. R. Forrest, Nat. Energy **3**, 422 (2018).

[2] Z. Zheng, Q. Hu, S. Zhang, D. Zhang, J. Wang, S. Xie, R. Wang, Y. Qin, W. Li, L. Hong, N. Liang, F. Liu, Y. Zhang, Z. Wei, Z. Tang, T. P. Russell, J. Hou, and H. Zhou, Adv. Mater. , 1801801 (2018).

[3] M. C. Scharber, D. Mühlbacher, M. Koppe, P. Denk, C. Waldauf, A. J. Heeger, and C. J. Brabec, Adv. Mater. **18**, 789 (2006).

[4] J. A. Bartelt, D. Lam, T. M. Burke, S. M. Sweetnam, and M. D. McGehee, Adv. Energy Mater. **5**, 1500577 (2015).

[5] D. Bartesaghi, I. D. C. Pérez, J. Kniepert, S. Roland, M. Turbiez, D. Neher, and L. J. A. Koster, Nat. Commun. **6**, 7083 (2015).

[6] I. Ramirez, M. Causa', Y. Zhong, N. Banerji, and M. Riede, Adv. Energy Mater. (2018), 10.1002/aenm.201701073.

[7] C. Göhler, A. Wagenpfahl, and C. Deibel, Adv. Electron. Mater. (2018), 10.1002/aelm.201700505.

[8] S. Shoaee, M. Stolterfoht, and D. Neher, Adv. Energy Mater. (2018), 10.1002/aenm.201703355.

[9] P. Langevin, Ann. Chim. Phys. **28**, 433 (1903).

[10] A. Pivrikas, G. Juška, A. J. Mozer, M. Scharber, K. Arlauskas, N. S. Sariciftci, H. Stubb, and R. Österbacka, Phys. Rev. Lett. **94**, 176806 (2005).

[11] T. M. Clarke, D. B. Rodovsky, A. A. Herzing, J. Peet, G. Dennler, D. DeLongchamp, C. Lungenschmied, and A. J. Mozer, Adv. Energy Mater. **1**, 1062 (2011).

[12] C. Groves and N. C. Greenham, Phys. Rev. B **78**, 155205 (2008).

[13] M. C. Heiber, C. Baumbach, V. Dyakonov, and C. Deibel, Phys. Rev. Lett. **114**, 136602 (2015).

[14] M. C. Heiber, T.-Q. Nguyen, and C. Deibel, Phys. Rev. B **93**, 205204 (2016).

[15] M. Hilczer and M. Tachiya, J. Phys. Chem. C **114**, 6808 (2010).

[16] A. J. Ferguson, N. Kopidakis, S. E. Shaheen, and G. Rumbles, J. Phys. Chem. C **115**, 23134 (2011).

[17] M. Ansari-Rad, G. Garcia-Belmonte, and J. Bisquert, Appl. Phys. Lett. **107**, 073301 (2015).

[18] T. M. Burke, S. Sweetnam, K. Vandewal, and M. D. McGehee, Adv. Energy Mater. **5**, 1500123 (2015).

[19] A. Armin, J. R. Durrant, and S. Shoaee, J. Phys. Chem. C **121**, 13969 (2017).

[20] V. Coropceanu, J.-L. Brédas, and S. Mehraeen, J. Phys. Chem. C **121**, 24954 (2017).

[21] T. M. Clarke, C. Lungenschmied, J. Peet, N. Drolet, and A. J. Mozer, Adv. Energy Mater. **5**, 1401345 (2015).

[22] D. Kiermasch, A. Baumann, M. Fischer, V. Dyakonov, and K. Tvingstedt, Energy Environ. Sci. **11**, 629 (2018).

[23] A. J. Mozer, G. Dennler, N. S. Sariciftci, M. Westerling, A. Pivrikas, R. Österbacka, and G. Juška, Phys. Rev. B **72**, 035217 (2005).

[24] T. M. Clarke, J. Peet, P. Denk, G. Dennler, C. Lungenschmied, and A. J. Mozer, Energy Environ. Sci. **5**, 5241 (2012).

[25] I. A. Howard, F. Etzold, F. Laquai, and M. Kemerink, Adv. Energy Mater. **4**, 1301743 (2014).

[26] J. Kurpiers and D. Neher, Sci. Rep. **6**, 26832 (2016).

[27] G. Zhang, T. M. Clarke, and A. J. Mozer, J. Phys. Chem. C **120**, 7033 (2016).

[28] C. G. Shuttle, B. O'Regan, A. M. Ballantyne, J. Nelson, D. D. C. Bradley, and J. R. Durrant, Phys. Rev. B **78**, 113201 (2008).

[29] A. Foertig, A. Baumann, D. Rauh, V. Dyakonov, and C. Deibel, Appl. Phys. Lett. **95**, 052104 (2009).

[30] A. Maurano, R. Hamilton, C. G. Shuttle, A. M. Ballantyne, J. Nelson, B. O'Regan, W. Zhang, I. McCulloch, H. Azimi, M. Morana, C. J. Brabec, and J. R. Durrant, Adv. Mater. **22**, 4987 (2010).

[31] D. Rauh, C. Deibel, and V. Dyakonov, Adv. Funct. Mater. **22**, 3371 (2012).

[32] A. Foertig, J. Kniepert, M. Gluecker, T. Brenner, V. Dyakonov, D. Neher, and C. Deibel, Adv. Funct. Mater. **24**, 1306 (2014).

[33] J. Gorenflot, M. C. Heiber, A. Baumann, J. Lorrmann, M. Gunz, A. Kämpgen, V. Dyakonov, and C. Deibel, J. Appl. Phys. **115**, 144502 (2014).

[34] Y. Firdaus, L. P. Maffei, F. Cruciani, M. A. Müller, S. Liu, S. Lopatin, N. Wehbe, G. O. N. Ndjawa, A. Amassian, F. Laquai, and P. M. Beaujuge, Adv. Energy Mater. **7**, 1700834 (2017).

[35] B. Wright, Y. Nakajima, T. M. Clarke, K. Okuda, H. Paananen, A. J. Mozer, and S. Mori, Adv. Energy Mater. **7**, 1602026 (2017).

[36] S. Albrecht, W. Schindler, J. Kurpiers, J. Kniepert, J. C. Blakesley, I. Dumsch, S. Allard, K. Fostiropoulos, U. Scherf, and D. Neher, J. Phys. Chem. Lett. **3**, 640 (2012).

[37] A. Melianas, F. Etzold, T. J. Savenije, F. Laquai, O. Inganäs, and M. Kemerink, Nat. Commun. **6**, 8778 (2015).

[38] A. Melianas, V. Pranculis, Y. Xia, N. Felekidis, O. Inganäs, V. Gulbinas, and M. Kemerink, Adv. Energy Mater. **7**, 1602143 (2017).

[39] J. C. Blakesley, F. A. Castro, W. Kylberg, G. F. A. Dibb, C. Arantes, R. Valaski, M. Cremona, J. S. Kim, and J.-S. Kim, Org. Electron. **15**, 1263 (2014).

[40] See Supplemental Material at [URL] for additional details and supplementary results.

[41] S. Albrecht, J. R. Tumbleston, S. Janietz, I. Dumsch, S. Allard, U. Scherf, H. Ade, and D. Neher, J. Phys. Chem. Lett. **5**, 1131 (2014).

[42] F. Fabregat-Santiago, G. Garcia-Belmonte, I. Mora-Seró, and J. Bisquert, Phys. Chem. Chem. Phys. **13**, 9083 (2011).

[43] G. Garcia-Belmonte, P. P. Boix, J. Bisquert, M. Sessolo, and H. J. Bolink, Sol. Energ. Mat. Sol. C. **94**, 366 (2010).

[44] L. Xu, J. Wang, Y.-J. Lee, and J. W. P. Hsu, J. Phys. Chem. C **119**, 19628 (2015).

[45] J. I. Basham, T. N. Jackson, and D. J. Gundlach, Adv. Energy Mater. **4**, 1400499 (2014).

[46] C. M. Proctor, C. Kim, D. Neher, and T.-Q. Nguyen, Adv. Funct. Mater. **23**, 3584 (2013).

[47] T. K. Mullenbach, Y. Zou, J. Holst, and R. J. Holmes, J. Appl. Phys. **116**, 124513 (2014).

[48] S. D. Collins, C. M. Proctor, N. A. Ran, and T.-Q. Nguyen, Adv. Energy. Mater. (2016), 10.1002/aenm.201501721.

[49] V. V. Brus, C. M. Proctor, N. A. Ran, and T.-Q. Nguyen, Adv. Energy Mater. **6**, 1502250 (2016).

[50] G. Garcia-Belmonte, A. Munar, E. M. Barea, J. Bisquert, I. Ugarte, and R. Pacios, Org. Electron. **9**, 847 (2008).

[51] J. Bisquert, L. Bertoluzzi, I. Mora-Sero, and G. Garcia-Belmonte, J. Phys. Chem. C **118**, 18983 (2014).

[52] S. Chen, S.-W. Tsang, T.-H. Lai, J. R. Reynolds, and F. So, Adv. Mater. **26**, 6125 (2014).

[53] N. Cho, C. W. SChlenker, K. M. Knesting, P. Koelsch, H.-L. Yip, D. S. Ginger, and A. K.-Y. Jen, Adv. Energy Mater. **4**, 1301857 (2014).

[54] G. F. A. Dibb, T. Kirchartz, D. Credgington, J. R. Durrant, and J. Nelson, J. Phys. Chem. Lett. **2**, 2407 (2011).

[55] M. Stolterfoht, S. Shoaee, A. Armin, H. Jin, I. Kassal, W. Jiang, P. Burn, and P. Meredith, Adv. Energy Mater. **7**, 1601379 (2017).

[56] A. K. Thakur, G. Wantz, G. Garcia-Belmonte, J. Bisquert, and L. Hirsch, Sol. Energ. Mat. Sol. C. **95**, 2131 (2011).

[57] A. K. Thakur, H. Baboz, G. Wantz, J. Hodgkiss, and L. Hirsch, J. Appl. Phys. **112**, 044502 (2012).

[58] T. M. Clarke, C. Lungenschmied, J. Peet, N. Drolet, K. Sunahara, A. Furube, and A. J. Mozer, Adv. Energy Mater. **3**, 1473 (2013).

[59] A. Baumann, K. Tvingstedt, M. C. Heiber, S. Väth, C. Momblona, H. J. Bolink, and V. Dyakonov, APL Mater. **2**, 081501 (2014).

[60] K. S. Rao and Y. N. Mohapatra, Appl. Phys. Lett. **104**, 203303 (2014).

[61] N. A. Ran, J. A. Love, M. C. Heiber, X. Jiao, M. P. Hughes, A. Karki, M. Wang, V. V. Brus, H. Wang, D. Neher, H. Ade, G. C. Bazan, and T.-Q. Nguyen, Adv. Energy Mater. **8**, 1701073 (2018).

[62] M. M. Mandoc, F. B. Kooistra, J. C. Hummelen, B. de Boer, and P. W. M. Blom, Appl. Phys. Lett. **91**, 263505 (2007).

[63] S. R. Cowan, A. Roy, and A. J. Heeger, Phys. Rev. B **82**, 245207 (2010).

[64] J. C. Blakesley and D. Neher, Phys. Rev. B **84**, 075210 (2011).

[65] I. Lange, J. Kniepert, P. Pingel, I. Dumsch, S. Allard, S. Janietz, U. Scherf, and D. Neher, J. Phys. Chem. Lett. **4**, 3865 (2013).

[66] F. Padinger, R. S. Rittberger, and N. S. Sariciftci, Adv. Funct. Mater. **13**, 85 (2003).

[67] M. T. Dand, L. Hirsch, and G. Wantz, Adv. Mat. **23**, 3597 (2011).

[68] Y. Liang, J. Xia, S.-T. Tsai, Y. Wu, G. Li, C. Ray, and L. Yu, Adv. Mater. **22**, E135 (2010).

[69] L. Lu and L. Yu, Adv. Mater. **26**, 4413 (2014).

[70] S.-H. Liao, H.-J. Jhuo, Y.-S. Cheng, and S.-A. Chen, Adv. Mater. **25**, 4766 (2013).

[71] T. L. Nguyen, H. Choi, S.-J. Ko, M. A. Uddin, B. Walker, S. Yum, J.-E. Jeong, M. H. Yun, T. J. Shin, S. Hwang, J. Y. Kim, and H. Y. Woo, Energy. Environ. Sci. **7**, 3040 (2014).

[72] S.-J. Ko, B. Walker, T. L. Nguyen, H. Choi, J. Seifter, M. A. Uddin, T. Kim, S. Kim, J. Heo, G.-H. Kim, S. Cho, A. J. Heeger, H. Y. Woo, and J. Y. Kim, Adv. Funct. Mater. **26**, 3324 (2016).

[73] M. Wang, H. Wang, T. Yokoyama, X. Liu, Y. Huang, Y. Zhang, T.-Q. Nguyen, S. Aramaki, and G. C. Bazan, J. Am. Chem. Soc. **136**, 12576 (2014).

[74] C. G. Shuttle, R. Hamilton, J. Nelson, B. C. O'Regan, and J. R. Durrant, Adv. Funct. Mater. **20**, 698 (2010).

[75] J. Kniepert, I. Lange, N. J. van der Kaap, L. J. A. Koster, and D. Neher, Adv. Energy Mater. **4**, 1301401 (2014).

[76] F. Deledalle, P. S. Tuladhar, J. Nelson, J. R. Durrant, and T. Kirchartz, J. Phys. Chem. C **118**, 8837 (2014).

[77] J. Kniepert, I. Lange, J. Heidbrink, J. Kurpiers, T. J. K. Brenner, L. J. A. Koster, and D. Neher, J. Phys. Chem. C **119**, 8310 (2015).

[78] N. Gasparini, X. Jiao, T. Heumueller, D. Baran, G. J. Matt, S. Fladischer, E. Spiecker, H. Ade, C. J. Brabec, and T. Ameri, Nature Energy **1**, 16118 (2016).

[79] S. B. Jo, M. Kim, D. H. Sin, J. Lee, H. G. Kim, H. Ko, and K. Cho, Adv. Energy Mate. **5**, 1500802 (2015).

[80] P. Kaienburg, U. Rau, and T. Kirchartz, Phys. Rev. Appl. **6**, 024001 (2016).

[81] C. M. Proctor, J. A. Love, and T.-Q. Nguyen, Adv. Mater. **26**, 5957 (2014).

[82] B. A. Collins, J. R. Tumbleston, and H. Ade, J. Phys. Chem. Lett. **2**, 3135 (2011).

[83] F. C. Jamieson, E. B. Domingo, T. McCarthy-Ward, M. Heeney, N. Stingelin, and J. R. Durrant, Chem. Sci.

3, 485 (2012).

[84] S. Shoaee, S. Subramaniyan, H. Xin, C. Keiderling, P. S. Tuladhar, F. Jamieson, S. A. Jenekhe, and J. R. Durrant, Adv. Funct. Mater. **23**, 3286 (2013).

[85] S. Sweetnam, K. R. Graham, G. O. N. Ndjawa, T. Heumüller, J. A. Bartelt, T. M. Burke, W. Li, W. You, A. Amassian, and M. D. McGehee, J. Am. Chem. Soc. **136**, 14078 (2014).

[86] B. A. Collins, Z. Li, J. R. Tumbleston, E. Gann, C. R. McNeill, and H. Ade, Adv. Energy. Mater. **3**, 65 (2013).

[87] S. Roland, M. Schubert, B. A. Collins, J. Kurpiers, Z. Chen, A. Facchetti, H. Ade, and D. Neher, J. Phys. Chem. Lett. **5**, 2815 (2014).

[88] S. Mukherjee, C. M. Proctor, G. C. Bazan, T.-Q. Nguyen, and H. Ade, Adv. Energy Mater. **5**, 1500877 (2015).

[89] S. Engmann, H. W. Ro, A. A. Herzing, D. M. De-Longchamp, C. R. Snyder, L. J. Richter, A. Barito, and D. J. Gundlach, J. Mater. Chem. A **5**, 6893 (2017).

[90] L. Ye, H. Hu, M. Ghasemi, T. Wang, B. A. Collins, J.-H. Kim, K. Jiang, J. H. Carpenter, H. Li, Z. Li, T. McAfee, J. Zhao, X. Chen, J. L. Y. Lai, T. Ma, J.-L. Bredas, H. Yan, and H. Ade, Nat. Mater. **17**, 253 (2018).

[91] M. C. Heiber, K. Kister, A. Baumann, V. Dyakonov, C. Deibel, and T.-Q. Nguyen, Phys. Rev. Appl. **8**, 054043 (2017).

[92] M. Obarowska and J. Godlewski, Synthetic Met. **109**, 219 (2000).

[93] N. Gasparini, M. Salvador, T. Heumueller, M. Richter, A. Classen, S. Shrestha, G. J. Matt, S. Holliday, S. Strohm, H.-J. Egelhaaf, A. Wadsworth, D. Baran, I. McCulloch, and C. J. Brabec, Adv. Energy Mater.

[94] K. Sun, Z. Xiao, S. Lu, W. Zajaczkowski, W. Pisula, E. Hanssen, J. M. White, R. M. Williamson, J. Subbiah, J. Ouyang, A. B. Holmes, W. W. H. Wong, and D. J. Jones, Nat. Commun. **6**, 6013 (2015).

[95] P. Cai, Z. Chen, L. Zhang, J. Chen, and Y. Cao, J. Mater. Chem. C **5**, 2786 (2017).

[96] Q. Fan, Y. Wang, M. Zhang, B. Wu, X. Guo, Y. Jiang, W. Li, B. Guo, C. Ye, W. Su, J. Fang, X. Ou, F. Liu, Z. Wei, T. C. Sum, T. P. Russell, and Y. Li, Adv. Mater. **30**, 1704546 (2017).

[97] B. Guo, W. Li, X. Guo, X. Meng, W. Ma, M. Zhang, and Y. Li, Adv. Mater. **29**, 1702291 (2017).

[98] Y. Jin, Z. Chen, M. Xiao, J. Peng, B. Fan, L. Ying, G. Zhang, X.-F. Jiang, Q. Yin, Z. Liang, F. Huang, and Y. Cao, Adv. Energy Mater. **7**, 1700944 (2017).

[99] X. Liu, L. Nian, K. Gao, L. Zhang, L. Qing, Z. Wang, L. Ying, Z. Xie, Y. Ma, Y. Cao, F. Liu, and J. Chen, J. Mater. Chem. A **5**, 17619 (2017).

[100] J. Hachmann, R. Olivares-Amaya, A. Jinich, A. L. Appleton, M. A. Blood-Forsythe, L. R. Seress, C. Román-Salgado, K. Trepte, S. Atahan-Evrenk, S. Er, S. Shrestha, R. Mondal, A. Sokolov, Z. Bao, and A. Aspuru-Guzik, Energy Environ. Sci. **7**, 698 (2014).

[101] Y. Imamura, M. Tashiro, M. Katouda, and M. Hada, J. Phys. Chem. C **121**, 28275 (2017).

[102] S. A. Lopez, B. Sanchez-Lengeling, J. de Goes Soares, and A. Aspuru-Guzik, Joule **1**, 857 (2017).

[103] H. Sahu, W. Rao, A. Troisi, and H. Ma, Adv. Energy Mater. , 1801032 (2018).

7, 1701561 (2017).